Bowtie nano-aperture as interface between near-fields and a single-mode fiber

M. Mivelle[1,2,*]**, I.A. Ibrahim**[1]**, F. Baida**[1]**, G.W. Burr**[2]**, D. Nedeljkovic**[3]**, D. Charraut**[1]**, J-Y. Rauch**[1]**, R. Salut**[1]**, T. Grosjean**[1]

[1] *Département d'Optique P.M. Duffieux,*
Institut FEMTO-ST, UMR CNRS 6174, Université de Franche-Comté,
16 route de Gray, 25030 Besançon cedex, France

[2] *IBM Almaden Research Center, D2/K13E,*
650 Harry Road, San Jose, California 95120, USA

[3] *Lovalite s.a.s.*
18 rue Alain Savary, 25000 Besançon
[*]*mathieu.mivelle@femto-st.fr*

Abstract: We present the development and study of a single bowtie nano-aperture (BNA) at the end of a monomode optical fiber as an interface between near-fields/nano-optical objects and the fiber mode. To optimize energy conversion between BNA and the single fiber mode, the BNA is opened at the apex of a specially designed polymer fiber tip which acts as an efficient mediator (like a horn optical antenna) between the two systems. As a first application, we propose to use our device as polarizing electric-field nanocollector for scanning near-field optical microscopy (SNOM). However, this BNA-on-fiber probe may also find applications in nanolithography, addressing and telecommunications as well as in situ biological and chemical probing and trapping.

© 2010 Optical Society of America

References and links

1. P. Mühlschlegel, H.-J. Eisler, O. Martin, B. Hecht, and D. Pohl, "Resonnant optical antenna," Science **308**, 1607–1609 (2005).
2. R. Grober, R. Schoelkopf, and D. Prober, "Optical antenna: Towards a unity efficiency near-field optical probe," Appl. Phys. Lett. **70**(11), 1354–6 (1997).
3. P. Schuck, D. Fromm, A. Sundaramurthy, G. Kino, and W. Moerner, "Improving the mismatch between light and nanoscale objects with gold bowtie nanoantennas," Phys. Rev. Lett. **94**, 017402 (2005).
4. T. Taminiau, R. Moerland, F. Segerink, L. Kuipers, and N. V. Hulst, "$\lambda/4$ resonance of an optical monopole antenna probes by single molecule fluorescence," Nano Lett. **7**, 28 (2007).
5. L. Wang, S. Uppuluri, E. Jin, and X. Xu, "Nanolithography using high transmission nanoscale bowtie apertures," Nano Lett. **6**, 361 (2006).
6. T. Kalkbrenner, U. Hakanson, A. Schädle, S. Burger, C. Henkel, and V. Sandoghdar, "Optical microscopy via spectral modifications of a nano-antenna," Phys. Rev. Lett. **95**(20), 200801.1–4 (2005).
7. A. Alù and N. Engheta, "Hertzian plasmonic nanodimer as an efficient optical nanoantenna," Phys. Rev. B **78**(19), 195111 (2008).

8. A. Kinkhabwala, Z. Yu, S. Fan, Y. Avlasevich, K. Mullen, and W. E. Moerner, "Large single-molecule fluorescence enhancements produced by a bowtie nanoantenna," Nat. Photon. **3**, 654–657 (2009).

9. P. Anger, P. Bharadwaj, and L. Novotny, "Enhancement and Quenching of Single-Molecule Fluorescence," Phys. Rev. Lett. **96**(11), 113002 (2006).

10. J. Farahani, D. Pohl, H.-J. Eisler, and B. Hecht, "Single quantum dot coupled to a scanning optical antenna : A tunable superemitter," Phys. Rev. Lett. **95**(1), 017402.1–4 (2005).

11. A. Sundaramurthy, P. J. Schuck, N. Conley, D. Fromm, G. Kino, and W. Moerner, "Toward Nanometre-Scale Optical photolithography: utilizing the near-field of bowtie optical nanoantennas," Nano Lett. **6**, 355 (2006).

12. N. Murphy-DuBay, L. Wang, E. C. Kinzel, S. M. V. Uppuluri, and X. Xu, "Nanopatterning using NSOM probes integrated with high transmission nanoscale bowtie aperture," Opt. Express **16**(4), 2584–2589 (2008).

13. M. Righini, P. Ghenuche, S. Cherukulappurath, V. Myroshnychenko, F. G. de Abajo, and R. Quidant, "Nano-optical trapping of Rayleigh particles and escherichia coli bacteria with resonant optical antennas," Nano Lett. **9**, 3387–3391 (2009).

14. P. Biagioni, M. Savoini, J. Huang, L. Duò, M. Finazzi, and B. Hecht, "Near-field polarization shaping by a near-resonant plasmonic cross antenna," Phys. Rev. B **80**(15), 153409 (2009).

15. T. Hanke, G. Krauss, D. Träutlein, B. Wild, R. Bratschitsch, and A. Leitenstorfer, "Efficient Nonlinear Light Emission of Single Gold Optical Antennas Driven by Few-Cycle Near-Infrared Pulses," Phys. Rev. Lett. **103**(25), 257404 (2009).

16. M. Danckwerts and L. Novotny, "Optical Frequency Mixing at Coupled Gold Nanoparticles," Phys. Rev. Lett. **98**(2), 026104 (2007).

17. L. Novotny, D. Pohl, and P. Regli, "Light propagation through nanometer-sized structures: the two-dimensional-aperture scanning near-field optical microscope," J. Opt. Soc. Am. A **11**, 1768–1779 (1994).

18. E. Smythe, E. Cubukcu, and F. Capasso, "Optical properties of surface plasmon resonances of coupled metallic nanorods," Opt. Express **15**(12), 7439–7447 (2007).

19. D. Chang, A. Sørensen, P. Hemmer, and M. Lukin, "Quantum Optics with Surface Plasmons," Phys. Rev. Lett. **97**(5), 053002.

20. I. Ibrahim, M. Mivelle, T. Grosjean, J.-T. Allegre, G. Burr, and F. Baida, "The bowtie shaped nano-aperture: a modal study," Accepted.

21. A. Taflove and S. Hagness, *Computational Electrodynamics: The Finite-Difference Time-Domain Method, Third Edition* (Artech House, Boston, 2005).

22. J. Roden and S. Gedney, "Convolution PML (CPML): an efficient fdtd implementation of the CFS-PML for arbitrarymedia," Microw. Opt. Technol. Lett **27**, 334–339 (2000).

23. J.-S. Huang, J. Kern, P. Geisler, P. Weinmann, M. Kamp, A. Forchel, P. Biagioni, and B. Hecht, "Mode imaging and selection in strongly coupled nanoantennas," Nano Lett., To be published .

24. T. Grosjean, M. Mivelle, and G. W. Burr, "Polarization-dependent extraction properties of bare fiber probes," Opt. Lett. **35**(3), 357–359 (2010).

25. L. Novotny and B. Hecht, *Principle of nano-optics* (Cambridge University Press, 2006).

26. R. Bachelot, C. Ecoffet, D. Deloeil, P. Royer, and D.-J. Lougnot, "Integration of Micrometer-Sized Polymer Elements at the End of Optical Fibers by Free-Radical Photopolymerization," Appl. Opt. **40**, 5860–5871 (2001).

27. L. Novotny, M. Beversluis, K. Youngworth, and T. Brown, "Longitudinal field modes probed by single molecules," Phys. Rev. Lett. **86**(23), 5251 (2001).

28. L. Wang and X. Xu, "High transmission nanoscale bowtie-shaped aperture probe for near-field optical imaging," Appl. Phys. Lett. **90**, 261105 (2007).

29. E. Betzig, J. K. Trautman, J. S. Weiner, T. D. Harris, and R. Wolfe, "Polarization contrast in near-field scanning optical microscopy," Appl. Opt. **31**(22), 4563–4568 (1992).

30. K. Lee, H. Kihm, J. Kihm, W. Choi, H. Kim, C. Ropers, D. Park, Y. Yoon, S. Choi, D. Woo, J. Kim, B. Lee, Q. Parka, C. Lienau, and D. Kim, "Vector field microscopic imaging of light," Nat. Photon. **1**, 53–56 (2007).

31. M. Burresi, D. van Oosten, T. Kampfrath, H. Schoenmaker, R. Heideman, A. Leinse, and L. Kuipers, "Probing the Magnetic Field of Light at Optical Frequencies," Science **326**, 550–553 (2009).

32. T. Grosjean, I. A. Ibrahim, M. A. Suarez, G. W. Burr, M. Mivelle, and D. Charraut, "Full vectorial imaging of electromagneticlight at subwavelength scale," Opt. Express **18**(6), 5809–5824 (2010).

33. E. Bortchagovsky, G. C. des Francs, D. Molenda, A. Naber, and U. Fischer, "Transmission of an obliquely incident beam of light through small apertures in a metal film," Appl. Phys. B **84**, 49–53 (2006).

34. U. Schröter and A. Dereux., "Surface plasmon polaritons on metal cylinders with dielectric core." Phys. Rev. B. **64**, 125420.1–10 (2001).

1. Introduction

The improvement of nanoscale fabrication technologies has allowed the investigation of enhanced optical phenomena on metallic nanoparticles, leading to novel nanoantenna concepts, such as the dipole [1], bowtie [2, 3] and monopole nanoantennas [4] as well as bowtie nano-

apertures [5], single particles [6] and dimers [7]. Nanoantennas are now widely used to optically interconnect free-space propagating waves together with highly localized fields for applications in the enhancement and control of the fluorescence of single emitters [8–10], nanolithography [5, 11, 12], optical tweezing [13], near-field polarization engineering [14] and non-linear optics [15, 16].

Despite the large number of potential applications, the development of resonant nanoantennas as an optical interface between near-fields and diffraction-limited fiber modes has not been extensively explored. A monopole nanoantenna has been grafted at the apex of a conventional fiber SNOM aperture tip to probe and control single molecule fluorescence [4]. The low throughput of the aperture tip which held the nanoantenna [17] was however a limiting factor of that system. A plasmonic fiber probe has been demonstrated for in situ surface enhanced Raman scattering (SERS) detection, with a matrix of nanoantennas engineered at the end facet of a cleaved multimode optical fiber [18]. Unfortunately, the uniform and optimized excitation of the nanoantenna array required for optimized non-local SERS measurements cannot be achieved with highly multimode in-fiber illumination. Finally, the efficient optical coupling of quantum emitters to optical waveguides has been proposed through the plasmon excitation of metallic nanowires and nanotips for applications in the generation of guided single photons on demand [19]. This technique, based on phase-matching between plasmon and waveguide modes, reaches very high coupling ratios but seems to be difficult to be implemented directly on a optical fiber.

In this paper, we propose to use a single bowtie nano-aperture (BNA) to interface diffraction-limited single-mode optical fibers with near-fields and nano-optical structures. To improve the nanoantenna-to-fiber optical coupling, the BNA is fabricated at the apex of a specially designed metal-coated tapered tip. The resulting nanoantenna fiber probe opens new perspectives in SNOM imaging, nanolithography, addressing and telecommunications as well as in situ biological and chemical probing and trapping. As a first application, we use this fiber probe as an integrated nanocollector for SNOM since it behaves as a high resolution polarizing nanocollector with little sensitivity to the magnetic optical field. This new setup may bring new opportunities to better discriminate between electric and magnetic fields in collection-mode SNOM for an improved image interpretation.

2.   Design and theoretical study of the device

2.1.   Design

The design of our nanoantenna fiber probe, shown schematically in Figure 1, consists of a single bowtie nano-aperture (BNA) opened at the end of a 30-micron long metal-coated fiber tip. A BNA and bowtie nanoantennas are complementary gap-based nanoantenna geometries which have similar capabilities for confining and enhancing optical radiations [3, 5]. However, a BNA has the ability to strongly reduce background signal, which is of great practical interest in the development of a highly-sensitive fiber nanoprobe that can be immersed in inhomogeneous diffusing media. The role of the tapered tip is to optically harness the nanoantenna to the fiber, serving as a tapered waveguide aimed at efficiently matching radiation from the BNA to the fiber mode, and vice versa. Its rounded apex (with 500nm radius-of-curvature) insures propagation of the guided mode all the way to the end of the tip where the BNA is located. Viewing the BNA as an optical waveguide [20], the tapered tip may be seen as an intermediate horn optical antenna which matches the electromagnetic impedances of the BNA and the fiber guided mode. The proposed hybrid combination BNA/fiber-tip leads to a highly efficient single-nanoantenna fiber probe, which remains effective even with relatively low fiber input powers or less-sensitive detectors.
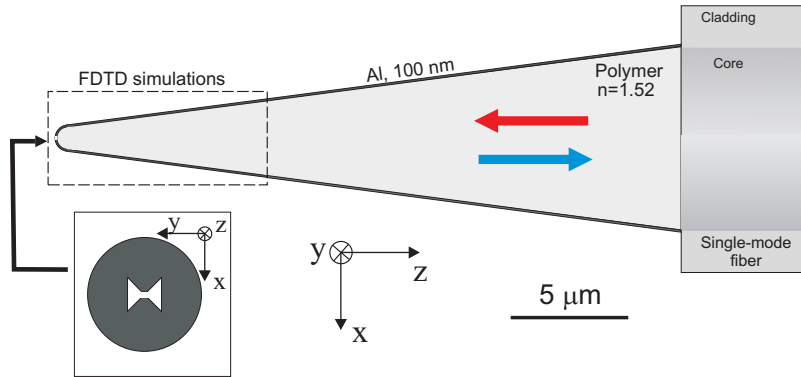
Fig. 1. Scheme of the proposed nanoantenna fiber device.

2.2. Theory

Using the Finite Difference Time Domain (FDTD) method [21], we have carried out a theoretical study of the optical response of the tip of the BNA fiber probe both in emission and collection modes. Although such investigations do not allow a quantitative study of the overall probe properties, they give a good idea about the probe performances and its appropriateness for integration onto an optical fiber. The model used for the simulation of the BNA-on-tip is depicted inside the dashed-line rectangle of Fig. 1, consisting of a volume spanning ± 2.3 μm in x and y about the tip apex. The refractive index and taper angle of the dielectric body of the tip are chosen to be equal to 1.52 and 15°, respectively. The tip is considered to be metal-coated with 100 nm of aluminum, whose dielectric constant is given by a Drude model. Aluminum is chosen for its high conductivity at infrared frequencies leading to high antenna effect. A 310 nm wide BNA with 45 nm wide square gap and 45° flare angles is opened at the rounded apex of the tip. The tip apex, with a radius of 500 nm, is located at x=y=z=0 and the simulation spans 1 micron below the tip in air, and terminates 9 microns into the body of the tip. All six boundaries of the computation volume are terminated with Convolutional-PMLs [22] in order to avoid parasitic unphysical reflections around the probe. The non-uniform grid resolution varies from 25nm for portions at the periphery of the simulation, to 5nm in the region immediately around the BNA ($\pm$ 190 nm in x and y and spanning -150 nm to 750 nm in z). Note that BNA geometry has been chosen so that it is resonant at $\lambda = 1.55$ microns, using a theoretical design procedure not detailed.

Figure 2 reports the simulation results of the BNA-on-tip in emission mode, when a gaussian beam is launched into the tip portion under study (excitation wavelength: $\lambda = 1.55$ microns). The waist of the input beam fits the entrance aperture of the tip on which it is projected. We show here the electric-field enhancement along the last 2 microns of the tip, in the (xz)-plane, ie., the ratio R between the intensity along the tip and the maximum input intensity. Figure insets display the electric enhancement in the transverse (xy)-plane placed 10 nm beyond the very tip. The incident polarization is (a,b) parallel and (c) perpendicular to the axis (0x) of the BNA metallic triangles. We clearly see in (b) and (c) ((b) displays the fifth root of R calculated in (a)), the cutoff-free guiding property of the tip apex which efficiently drives energy up to the BNA. The resulting intensity enhancement in the BNA gap, which is observed only in (a) and (b), is about 350. Therefore, large fields may be expected in the gap of the BNA even for relatively low power in the input fiber mode. The high polarization sensitivity of the BNA is due to its high asymmetric shape, which leads to a charge distribution in the gap zone corresponding

to an oscillating electric dipole. Such dipole properties are characteristics for the resonant mode which is strongly bound to the gap [2, 7, 23].
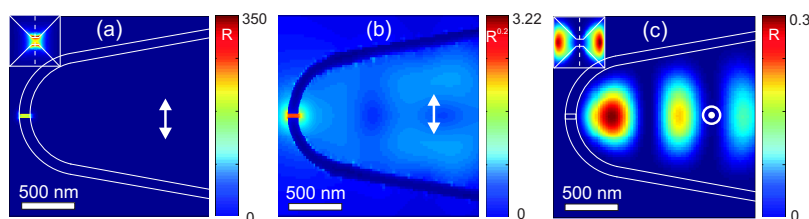

Fig. 2. Enhancement factor R of the optical electric field intensity ((xz)-plane) in the last 2 microns of the BNA fiber probe. R is the ratio between intensity in the tip apex and the maximum intensity of the input gaussian beam. The incident polarization is (a,b) parallel and (c) perpendicular to the direction (0x) of the BNA metal triangles. In (b), the color scale is mapped to R raised to the power 0.2, in order to provide a better view of the light distribution within the taper. Insets of (a) and (c) show R-factor in a transverse (xy)-plane placed 10 nm far from the BNA. Maximum values of R along this (xy)-plane are 120 in (a) and 1.5 in (c).

Following a reciprocal approach, we can investigate the collection properties of our system by studying the efficiency with which the BNA radiates light into the tip body when excited with electric and magnetic dipole moments located in the gap zone. Given the "emission" properties of gap antennas, the collection process can be assumed to be mainly driven by the excitation of the gap, which then resonantly induces the far-field radiation of the overall structure into the tip. A corresponding experiment would be the detection with our fiber probe of fluorescent single molecules.

Figures 3 (b) and (c) show the spectral response of the BNA-on-tip with electric and magnetic dipole excitations, respectively. In both figures, collection spectra are shown for single dipoles positioned 10 nm below the gap of the BNA, oriented along (0x), (0y) and (0z) and radiating a single temporal pulse (see Fig. 3 (a)). In each case, the time-varying Poynting vector flow is calculated inside the probe, integrated over a transverse cross-section located 4.6 microns far from the BNA. The spectrum of the collected power (P) is calculated by a simple Fourier-transform of this result and normalized by the power spectrum of the free radiating dipole in vacuum (P_0). Simulations reveal a strong BNA-to-dipole resonant coupling only for the electric dipole oriented along the BNA metallic triangles. This spectral behavior denotes a high overlap between radiation of the dipole parallel to (0x) and the eigenmode of the BNA at the origin of light transmission. Therefore, even in collection mode, optical response of the gap is close to that of an electric dipole oriented along the BNA main axis, thus verifying reciprocity for our nanoantenna device, at least at infrared frequencies. As a consequence, the BNA used in collection mode may be seen as a nanopolarizer. Further investigations (not detailed here) show that the interplay between the magnetic dipole and the BNA is mainly induced by an optical electric coupling. This result tends to confirm that the BNA is mainly sensitive to a single electric-field component with only a small sensitivity to the magnetic field.

Since transverse electric dipoles are well-coupled to single mode fibers through tapered tips [24], we can expect high optical sensitivities of the proposed overall fiber probe in collection mode. At the resonance frequency, a collection efficiency of 20% is predicted for a BNA excitation with a transverse dipole oriented along (0x) and positioned 10 nm beneath the gap. This rather large value, equivalent to the quantum yield [25] of a single fluorophore (quantum dot or fluorescent molecule) into the tip, shows that the BNA is a promising highly-sensitive
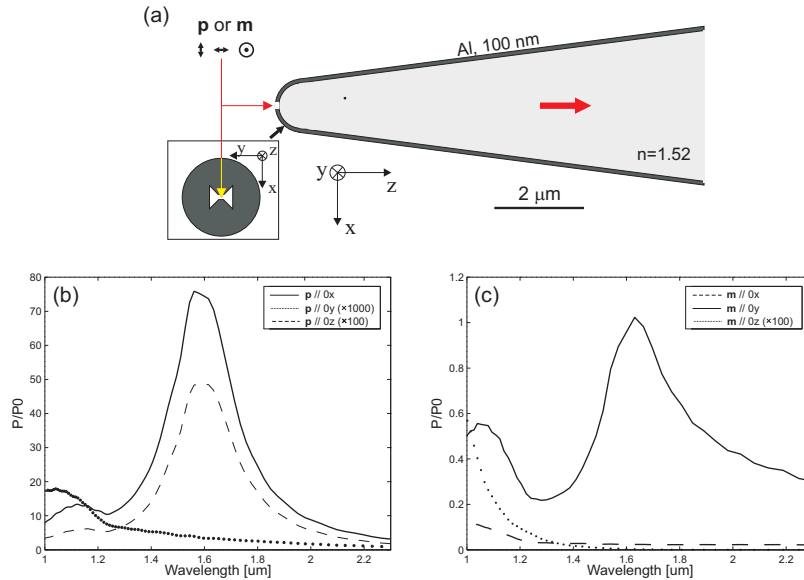
Fig. 3. (a): Scheme of the theoretical configuration. (b) and (c): collection spectra for tip excitations with (b) electric and (c) magnetic dipoles oriented along the 3 spatial directions.

optical nanoprobe, especially for interfacing single quantum emitters to optical fibers.

At the resonance frequency, the tip extraction efficiency is 170 fold larger with a dipole source oriented along (0x) than with the same dipole oriented along (0y), leading to a polarization ratio of 1:170. A non-local excitation of the BNA by plane waves leads to a polarization ratio of 1:37. This lower value is explained by a background effect due to the non negligible transmission of optical waves in the triangular apertures for the incident polarization along (0y). Therefore, the polarization ratio of the BNA-on-tip strongly depends on the kind of nano-object that is probed. Both polarization sensitivity and resolution can be strongly improved by reducing the gap width. Further investigations have shown that the polarization ratio of the BNA is enhanced to values around 1:30000 with a gap size of 5 nm for dipole excitation.

3. Fabrication and characterization

The fabrication procedure of BNA fiber probes is divided in three steps. First, polymer tips are optically grown at the cleaved end facet of a monomode (1.55 micron wavelength) glass fiber [26]. The on-fiber polymer technology developed by Lovalite company offers unique possibility to engineer complex shaped tapered fiber tips for optimum coupling conditions between the nanoantenna and the fiber. Even without metal cover, the high index difference between polymer tip and air is responsible for a high guiding effect throughout the tip,, from the fiber to the tip apex, and vice-versa. The excellent phase-matching between the fiber and tip-guided modes is due to the self-aligned fabrication procedure, in which a photosensitive mixture is polymerized directly by the fiber modes. Afterwards, the probes are metal coated with a few nanometer thick titanium adhesion layer followed by a 100 nm thick aluminum layer. Finally, the BNA of dimensions detailed in the theoretical section is opened by Focused Ion Beam (FIB) milling. Figures 4(a) and (b) display scanning electron micrographs of a resulting fiber device.

Figures 4 (c) and (d) show the far-field output of the BNA fiber probe used in emission mode, for incident guided fields with linear polarization parallel and perpendicular to the BNA
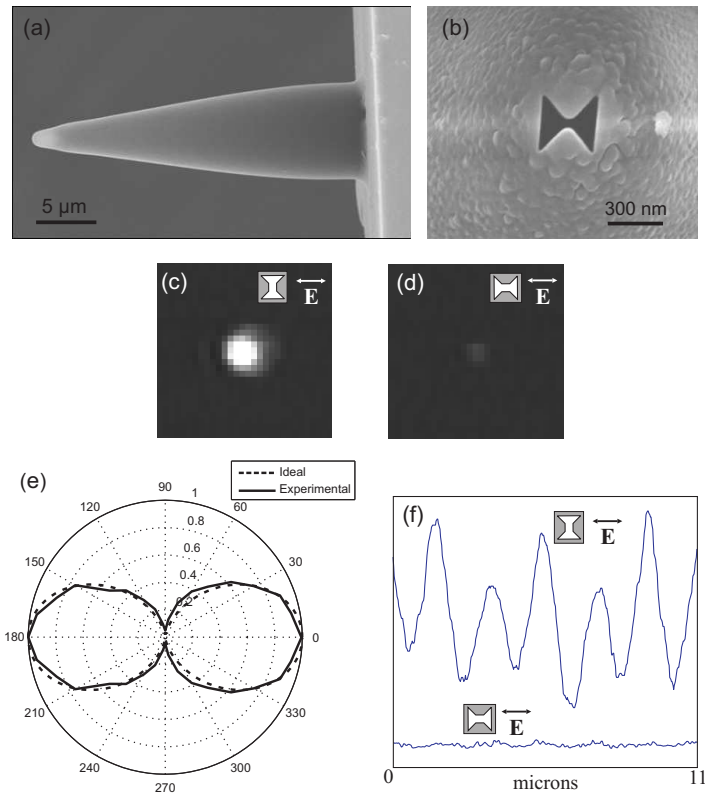
Fig. 4. (a,b) Scanning electron micrograph of the BNA fiber probe: (a) side view of the overall fiber tip and (b) top view of the tip apex revealing the BNA. (c,d) far-field radiation of the system used in emission mode, for input guided waves of orthogonal linear polarizations (see figure insets). (e) Polarization diagram of the BNA used in collection mode. Solid curve: experiments, dashed curve: case of an ideal nanopolarizer: fluorescence diagram of a single molecule (dipole absorption moment) versus incident polarization. (f) collected signals of the far-field diffraction pattern of a 1D-grating, for two orientations of the BNA with respect to the incident polarization (see figure insets).

metallic triangles (see figure insets), respectively. The BNA fiber nanosource is imaged with an objective (x100, 0.9 NA) coupled to an infrared camera (Hamamatsu), while a 100 μW linearly-polarized laser beam (λ=1.55 micron) is launched into the fiber through its free end facet. Because BNAs strongly limit background excitation fields, the antenna effect can be directly observed with a linear imaging process. The diffraction-limited bright spot visible when the incident polarization is oriented along the two metallic triangles of the nano-aperture almost vanishes when the polarization is rotated by 90°. This is in qualitative agreement with the field transmission shown in Fig. 2, which proves that our experimental device develops the expected dipolar antenna effect.

Figure 4 (e) displays the signal collected by the BNA fiber probe as a function of the incident polarization direction. This "polarization diagram" is measured by projecting a linearly-polarized collimated laser beam directly onto the BNA at normal incidence. Before reaching the probe, the laser beam passes through a half-wave plate to rotate the linear polarization at will. The fiber probe output is then connected to a conventional InGaAs amplified detector (Thorlabs). To ensure high signal-to-noise ratio, a synchronous detection scheme is used by modulating the input laser beam and connecting the detector to a lock-in amplifier (Stanford), which extracts the relevant signal at modulation frequency. The polarization diagram of the BNA is generated by measuring the collected signal through the probe while rotating the incident polarization over 360° by steps of 10°. This experimental result (Fig.4 (e), solid curve) is compared against the fluorescence of a single molecule (Fig.4 (e), dashed curve), which follows a sinusoidal law with respect to the direction of the incident polarization [27]. The good agreement between the two curves confirms that the collection properties of our experimental BNA fiber probe are mainly governed by an electric dipole moment parallel to the BNA metallic triangles. Our fiber device can thus be seen as a nanopolarizer with a polarization sensitivity of 1:31. This is close to the theoretical value 1:37 predicted in Section 2 with a large-scale plane-wave excitation. This polarization filtering performance is confirmed in Fig. 4(f), which shows the large scale spatial variations of the far-field diffraction pattern of a dielectric grating (period: 1.9 microns). The grating is illuminated in transmission mode at normal incidence with p-polarized waves (the incident electric field is perpendicular to the grooves). The collected signal, plotted along a single scan line perpendicular to the grating, is attenuated by 30 times when the BNA is rotated from the direction of the input polarization to the orthogonal one (as described by the figure insets).

4. BNA fiber probe for collection-mode SNOM

BNAs have already been used to enhance collection efficiency of SNOM systems [28]. Here, we suggest to exploit their high sensitivity to the electric field and polarization filtering properties to develop high-resolution local probes aimed at improving image contrast via polarization contrast technique [29], and to obtain a more detailed vectorial information about electromagnetic optical fields at subwavelength scale [30–32]. These BNA-on-fiber probes provide electric field information still inaccessible with rotationally-symmetric metal-coated aperture and aperture-less tips. Such conventional probes, which use ring-like metal patterns, are optically driven by both electric and magnetic dipole moments [33, 34], leading to high probe sensitivities for both electric and magnetic fields. This is a serious problem for accurate image interpretation, since in the presence of subwavelength spatial variations the electric and magnetic fields do not spatially overlap. Given its (electric) dipolar collection properties, the BNA fiber probe can bring innovative solution to this problem. Imaging of quantum emitters is also a highly promising application for these new probes.

We evaluate the ability of the BNA to accurately map nano-objects by computing the image accumulated by the probe during the scan of a single electric dipole (theoretical equivalent to a
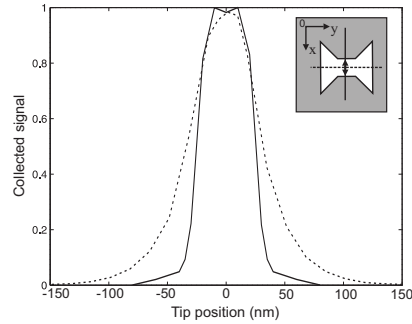
Fig. 5. Image with the BNA-on-tip of an electric dipole oriented along (0x) and placed 10 nm far from the BNA, in vacuum (represented by a double arrow in the figure inset). Solid curve: collected signal along (0x)-axis parallel to the BNA metallic triangles; dashed curve: collected signal along perpendicular (0y)-axis.

single molecule or a quantum dot). Figure 5 shows the image profiles resulting from the scan of the dipole along the two axis of symmetry of the BNA: the solid and dashed curves correspond to the axis parallel to (0x) and (0y) directions, respectively, with the dipole is oriented along the BNA metallic triangles (see figure inset). The dipole is positioned 10 nm beneath the probe, in air. In order to take into account tip-to-sample optical coupling, the dipole is positioned 10 nm over a dielectric flat substrate of optical index equal to 1.5. The images are obtained by calculating the collected power while varying the position of the tip by steps of a few nanometers along the two scan lines. The model of the probe and simulation parameters are identical to those used in section 2.2. We see that the image of the point-like source through the BNA is an elliptical spot whose full width at half-maximum, limited to 50 nm along (0x) and 80 nm along (0y), are bound to the 45 nm gap size and antenna shape. Following a conventional view of imaging, we can see in these spot dimensions the resolution ability of the BNA. Comparison of these results with the ones achieved without dielectric substrate shows that tip-to-sample coupling is (surprisingly) negligible. Note that both resolution and polarization performances are defined by the gap width of the BNA. Therefore, the higher the polarization ratio, the better the resolution.

A BNA fiber probe has been used to image a simple test-object: a 1D dielectric grating fabricated in a layer of PMMA with scanning electron beam lithography. The grating has a periodicity of 700 nm, a depth of 250 nm and a line-width of 200 nm. When this subwavelength-period grating is illuminated under normal incidence, all the diffracted orders in air are purely evanescent except zeroth order. Therefore, the field variations that include the contribution of the evanescent orders are located in the vicinity of the grating and are subwavelength in size. The acquisition set-up used here is typical for collection-mode SNOM. A linearly-polarized laser beam at the resonant wavelength of the BNA (λ=1.55 microns) is projected onto the grating at normal incidence through the back flat interface of the substrate (input waves are p-polarized). The BNA fiber probe is mounted in a commercial SNOM (from NTMDT company) that uses a shear force distance control to keep the BNA right at the grating surface (within 15 nm) during image acquisition. Images are formed by raster scanning the probe over the grating while collecting the optical signal which is guided toward a InGaAs amplified detector through the optical fiber. To ensure a satisfying signal-to-noise ratio, a conventional synchronous detection scheme as described earlier is implemented.

Figures 6(a) and (b) show topography and corresponding SNOM gray-scale image achieved
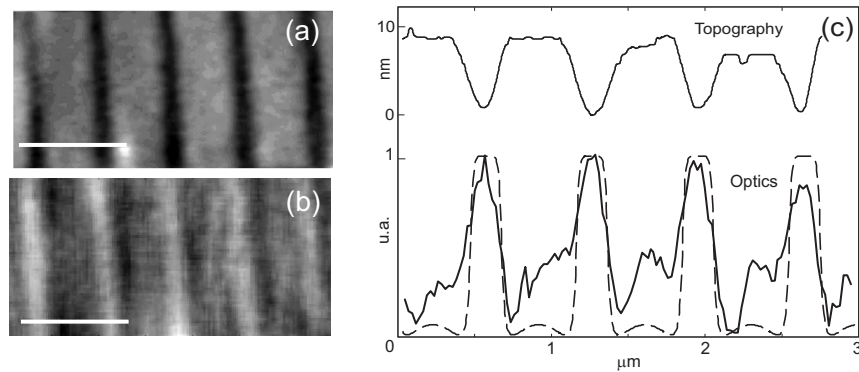
Fig. 6. (a): topography of the grating as measured by the BNA fiber probe, (b): corresponding optical image (scale bar: 1 micron), (c): upper curve: profile of the topography along a line perpendicular to the grooves, lower curves: profiles of the corresponding optical signal (solid line) and simulation of the intensity of the electric-field component along the BNA metallic triangles (perpendicular to the grating grooves) (dashed line).

with the BNA fiber probe, respectively. Here, the metal triangles of the BNA are oriented along the input polarization (perpendicular to the grating grooves). Figure 6(c) shows profiles of the topography (upper curve) and of the detected optical signal (lower curve, solid line). The optical signal is compared with the simulation of the intensity distribution of the transverse electric-field component parallel to the BNA triangles (dashed line). Theoretical results are achieved with a perfectly square grating whose geometrical parameters are described above. Good agreement between experiments and theory confirms that our fiber device is capable of faithfully probing the subwavelength variations of a single transverse component of the electric field, at least on dielectric surface. Asymmetry of the collected signal over a single period is probably due to either tip-to-sample coupling or to a slight BNA-to-tip decentring or tip asymmetry. Since the depth of the topography do not exceed 10 nm on a sample 25 times deeper, our BNA fiber tip acquires images in an almost constant-height regime. Note that the sharper variations of the collected signal occur over only 130 nm, roughly $\lambda/12$, arising from intensity variations at the grating edges that are predicted to span only 40nm in the near-field. Modulation of the detected signal are thus about 2.4 fold smaller than the aperture size, which confirms that the collection process is mainly initiated by the excitation of the gap of the BNA, rather than by a uniform transmission through the aperture.

5. Conclusion

We have proposed to use a single gap-nanoantenna (here, a BNA) to interface nano-optical phenomena and systems to diffraction-limited optical fibers. A prototype BNA fiber probe has been presented and its emission and collection properties have been numerically investigated. The results show that this integrated optical probe acts either as a tunable integrated nanosource which enhances light intensity by several hundred times and confines energy to a few cubic nanometers, or as a highly efficient nanocollector mainly sensitive to a single component of the electric optical near-fields. The fiber probe has been fabricated by FIB onto a polymer fiber tip and optically characterized in emission and collection modes. We found experimental results in good agreement with theoretical predictions. As first application, our system has been used as a polarizing electric-field nanocollector for SNOM. It may also find promising applications

in nanolithography, addressing and telecommunications, as well as in situ biological and chemical probing and trapping.